NASA TM X-181

TECHNICAL MEMORANDUM

X-181

EFFECT OF WING CRANK AND SWEEPBACK ON THE LOW SUBSONIC STABILITY AND CONTROL CHARACTERISTICS OF A MODEL OF A HYPERSONIC BOOST-GLIDE TYPE AIRPLANE

By Robert E. Shanks

Langley Research Center
Langley Field, Va.

NATIONAL AERONAUTICS AND SPACE ADMINISTRATION
WASHINGTON
February 1960

NATIONAL AERONAUTICS AND SPACE ADMINISTRATION

TECHNICAL MEMORANDUM X-181

EFFECT OF WING CRANK AND SWEEPBACK ON THE LOW SUBSONIC STABILITY AND CONTROL CHARACTERISTICS OF A MODEL OF A HYPERSONIC BOOST-GLIDE TYPE AIRPLANE*

By Robert E. Shanks

SUMMARY

A force test investigation has been made in the Langley free-flight tunnel to determine the effect of wing crank and sweepback on the low-subsonic stability and control characteristics of a model of a hypersonic boost-glide airplane having the fuselage and wing-tip fins on the upper surface of the wing. Static longitudinal and lateral stability and control data and rolling and yawing oscillation data are presented without analysis.

INTRODUCTION

An investigation is being conducted by the National Aeronautics and Space Administration to provide information on the stability and control characteristics of some proposed hypersonic boost-glide configurations over the speed range from hypersonic to low-subsonic speeds. The present investigation was made to provide some information at low-subsonic speeds on the longitudinal and lateral stability and control characteristics of a model having four different wing plan forms: two clipped delta wings and two cranked versions of clipped delta wings. A fuselage and wing-tip vertical tails were mounted on the upper surface of the wings.

The investigation was made over a range of angles of attack from 0° to 90° to determine the static longitudinal and lateral stability characteristics of all four configurations. The elevator and aileron effectiveness were determined from 0° to 30° angle of attack for one of the configurations. Also included in the investigation were rolling and yawing oscillation tests from 0° to 50° angle of attack to determine the oscillatory stability derivatives of two of the configurations.

DEFINITION OF TERMS AND SYMBOLS

The longitudinal data are referred to the wind axes. All lateral stability parameters and coefficients are referred to the body system of axes (see fig. 1) originating at a center-of-gravity position of 64 percent of the body length for all configurations except as noted. The term "in-phase derivative" used herein refers to any one of the stability derivatives which are based on the forces or moments in phase with the angle of roll or yaw produced in the oscillatory tests. The term "out-of-phase derivative" refers to any one of the stability derivatives which are based on the forces or moments 90° out of phase with the angle of roll or yaw. All measurements are reduced to standard coefficient form and are presented in terms of the following symbols:

X,Y,Z	body reference axes unless otherwise noted
S	wing area, sq ft
b	wing span, ft
$\bar{c}$	mean aerodynamic chord, ft
V	free-stream velocity, ft/sec
q	free-stream dynamic pressure, lb/sq ft
$\omega = 2\pi f$	radians/sec
f	frequency of oscillations, cps
k	reduced-frequency parameter, $\omega b/2V$
α	angle of attack, deg
β	angle of sideslip, deg or radians
r	yawing velocity, radians/sec
p	rolling velocity, radians/sec

$\dot{\beta} = \frac{d\beta}{dt}$

$\dot{r} = \frac{dr}{dt}$

$\dot{p} = \frac{dp}{dt}$

F_L lift, lb

F_D drag, lb

F_Y side force, lb

M_Y pitching moment, ft-lb

M_X rolling moment, ft-lb

M_Z yawing moment, ft-lb

C_m pitching-moment coefficient, $\frac{M_Y}{qS\bar{c}}$

C_l rolling-moment coefficient, $\frac{M_X}{qSb}$

C_n yawing-moment coefficient, $\frac{M_Z}{qSb}$

$C_{l_\beta} = \frac{\partial C_l}{\partial \beta}$ per radian

$C_{n_\beta} = \frac{\partial C_n}{\partial \beta}$ per radian

$C_{Y_\beta} = \frac{\partial C_Y}{\partial \beta}$ per radian

C_L lift coefficient, $\frac{F_L}{qS}$

C_D drag coefficient, $\frac{F_D}{qS}$

C_Y side-force coefficient, $\frac{F_Y}{qS}$

t time, sec

ϕ	angle of roll, radians
ψ	angle of yaw, radians
δ_e	elevator deflection, deg
δ_a	aileron deflections, $\delta_{a,R} - \delta_{a,L}$
$\delta_{a,R}, \delta_{a,L}$	right and left aileron deflection, respectively
W	wing
B	body
V	vertical tail

L
7
4
8

$$C_{l_r} = \frac{\partial C_l}{\partial \frac{rb}{2V}} \qquad C_{n_r} = \frac{\partial C_n}{\partial \frac{rb}{2V}} \qquad C_{Y_r} = \frac{\partial C_Y}{\partial \frac{rb}{2V}}$$

$$C_{l_p} = \frac{\partial C_l}{\partial \frac{pb}{2V}} \qquad C_{n_p} = \frac{\partial C_n}{\partial \frac{pb}{2V}} \qquad C_{Y_p} = \frac{\partial C_Y}{\partial \frac{pb}{2V}}$$

$$C_{l_{\dot{\beta}}} = \frac{\partial C_l}{\partial \frac{\dot{\beta}b}{2V}} \qquad C_{n_{\dot{\beta}}} = \frac{\partial C_n}{\partial \frac{\dot{\beta}b}{2V}} \qquad C_{Y_{\dot{\beta}}} = \frac{\partial C_Y}{\partial \frac{\dot{\beta}b}{2V}}$$

$$C_{l_{\dot{r}}} = \frac{\partial C_l}{\partial \frac{\dot{r}b}{2V}} \qquad C_{n_{\dot{r}}} = \frac{\partial C_n}{\partial \frac{\dot{r}b}{2V}} \qquad C_{Y_{\dot{r}}} = \frac{\partial C_Y}{\partial \frac{\dot{r}b}{2V}}$$

$$C_{l_{\dot{p}}} = \frac{\partial C_l}{\partial \frac{\dot{p}b}{2V}} \qquad C_{n_{\dot{p}}} = \frac{\partial C_n}{\partial \frac{\dot{p}b}{2V}} \qquad C_{Y_{\dot{p}}} = \frac{\partial C_Y}{\partial \frac{\dot{p}b}{2V}}$$

APPARATUS AND MODELS

The static and rotary oscillation tests were conducted in the Langley free-flight tunnel which is a low-speed tunnel with a 12-foot octagonal test section. Detailed descriptions of the oscillation apparatus and methods used in obtaining and reducing the data are given in reference 1. The model was sting mounted and the forces and moments were measured about the body axes by means of three-component internal strain-gage balances.

The model was constructed of aluminum alloy with the wings having a 1/8-inch flat-plate section. The same fuselage (B_1) and vertical tails (V_1) were used with each of the wings. The four different configurations are distinguished only by the difference in wing geometry as shown in figure 2 and the following table. Elevon control surfaces were cut for model $B_1W_4V_1$.

Wing	Area, sq in.	Span, in.	Aspect ratio
W_1	704.4	26.24	0.98
W_2	718.2	31.96	1.42
W_3	699.2	30.50	1.33
W_4	727.6	28.96	1.15

TESTS

The static longitudinal and lateral stability characteristics of the four configurations were determined for an angle-of-attack range of 0° to 90°. The lateral characteristics were determined from tests made at various angles of attack over a sideslip range of -20° to 20°. The elevator and aileron effectiveness were determined from 0° to 30° angle of attack for configuration $B_1W_4V_1$ only. Rolling and yawing oscillation tests were made over an angle-of-attack range from 0° to 50° for configurations $B_1W_1V_1$ and $B_1W_4V_1$. These oscillation tests were made at reduced-frequency values of 0.1 and 0.2. The rotary oscillation tests were made for amplitudes in roll and yaw of $\pm 5^\circ$.

The tests were made at a dynamic pressure of 4.25 pounds per square foot which corresponds to an airspeed of 60 feet per second and a test Reynolds number of 383,000 per foot and an average Reynolds number based on the model mean aerodynamic chord of approximately 1,000,000.

RESULTS

The results of the investigation are presented herein without discussion. The static longitudinal stability characteristics are presented in figure 3 for all four configurations. The pitching moments are referred to the 64-percent-body station in figure 3(a) and are referred to the 40-percent-mean-aerodynamic chord of the individual wings in figure 3(b). The longitudinal buildup characteristics for configuration $B_1W_1V_1$ are given in figure 4. The elevator effectiveness for configuration $B_1W_4V_1$ is given in figure 5. The variation of the lateral coefficients C_Y, C_n, and C_l with angle of sideslip β is presented in figures 6 to 9 for all four configurations. These data are summarized in figure 10 in the form of the variation of the derivatives C_{Y_β}, C_{n_β}, and C_{l_β} with angle of attack. The lateral derivatives were obtained by measuring the slope against sideslip of C_Y, C_n, and C_l between $\beta = -5^\circ$ and $\beta = 5^\circ$. Since some of these curves are nonlinear the data of figure 10 should be used only as an indication of the trends with angle of attack of the lateral stability near 0° sideslip. Aileron effectiveness data are presented in figure 11 for configurations $B_1W_4V_1$. The data obtained for configurations $B_1W_1V_1$ and $B_1W_4V_1$ from rolling and yawing oscillation tests are presented in figures 12 and 13, respectively.

Langley Research Center,
National Aeronautics and Space Administration,
Langley Field, Va., August 18, 1959.

REFERENCE

1. Hewes, Donald E.: Low-Subsonic Measurements of the Static and Oscillatory Lateral Stability Derivatives of a Sweptback-Wing Airplane Configuration at Angles of Attack From -10° to 90°. NASA MEMO 5-20-59L, 1959.

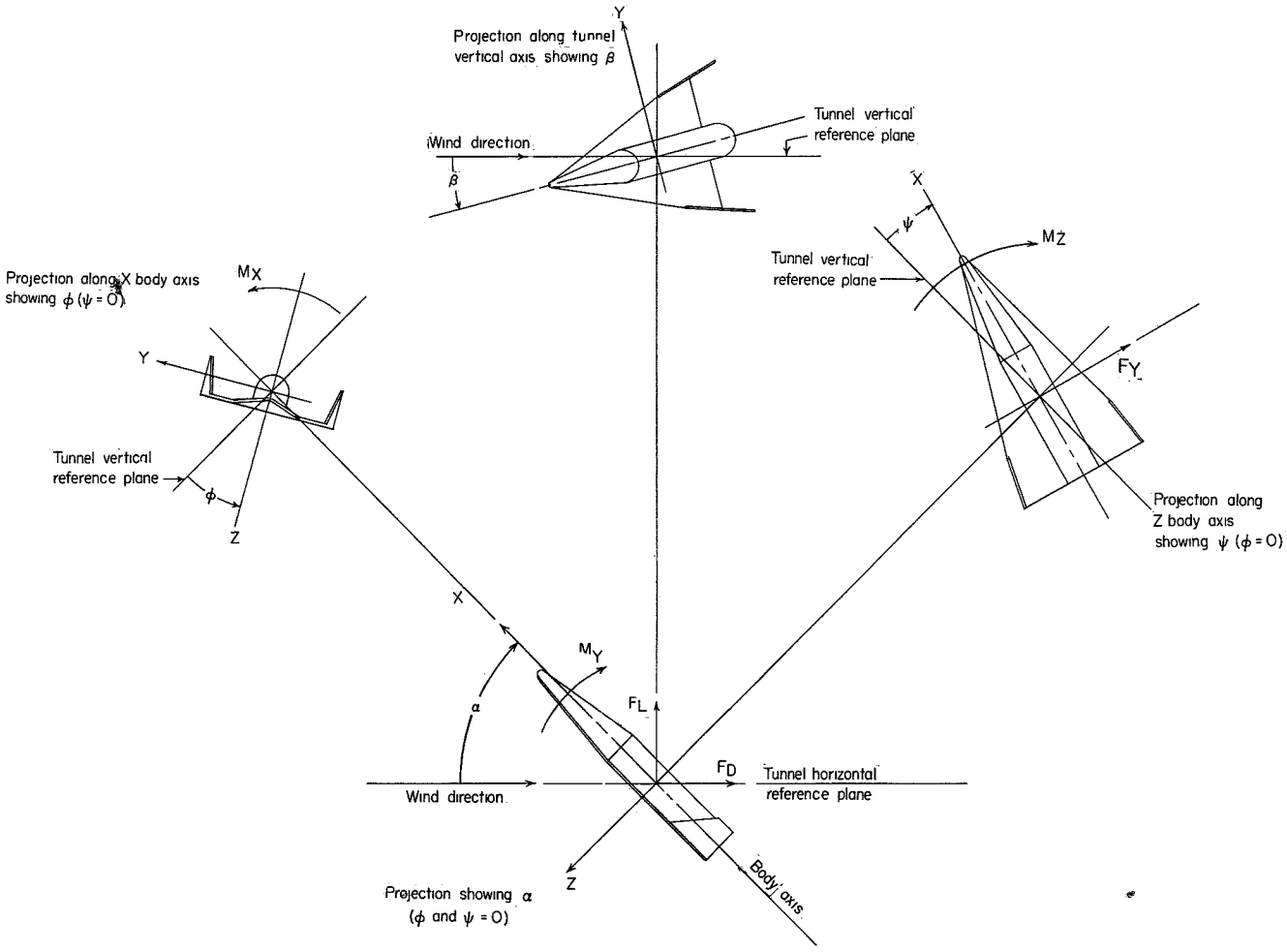

Figure 1.- The body system of axes. Arrows indicate positive directions of moments, forces, and angles. This system of axes is defined as an orthogonal system having the origin at the center of gravity and in which the X-axis is in the plane of symmetry and alined with the longitudinal axis of the fuselage, the Z-axis is in the plane of symmetry and perpendicular to the X-axis, and the Y-axis is perpendicular to the plane of symmetry.

Wing	Area, sq in.	Span, in.	Aspect Ratio	$\bar{c}$, in.	Moment reference, % $\bar{c}$
1	704.4	26.24	0.98	34.0	48.8
2	718.2	31.96	1.42	28.4	38.7
3	699.2	30.50	1.33	29.3	40.6
4	727.6	28.96	1.15	32.1	45.6

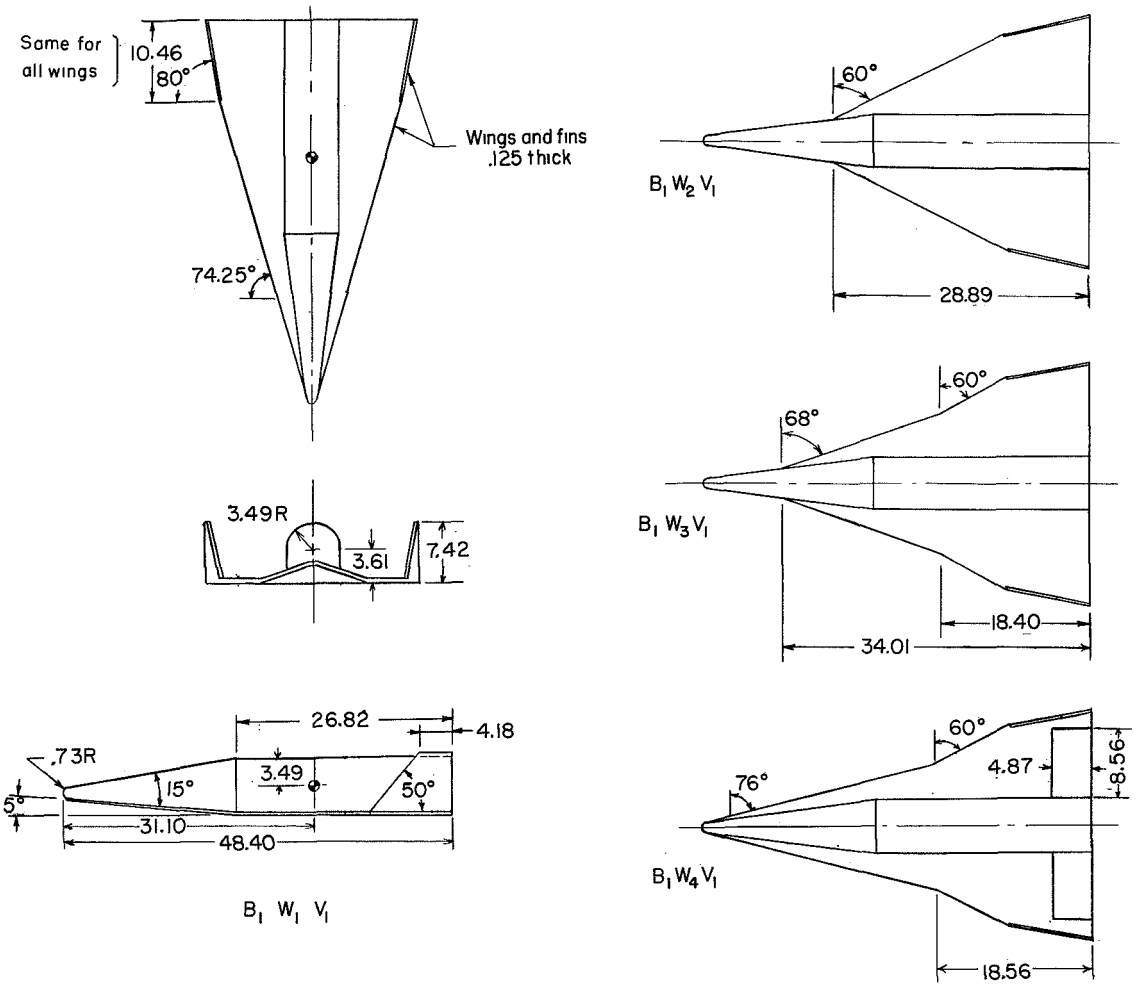

Figure 2.- Configurations of the model used in the investigation. Same fuselage and vertical tails used for all configurations. All dimensions are in inches.

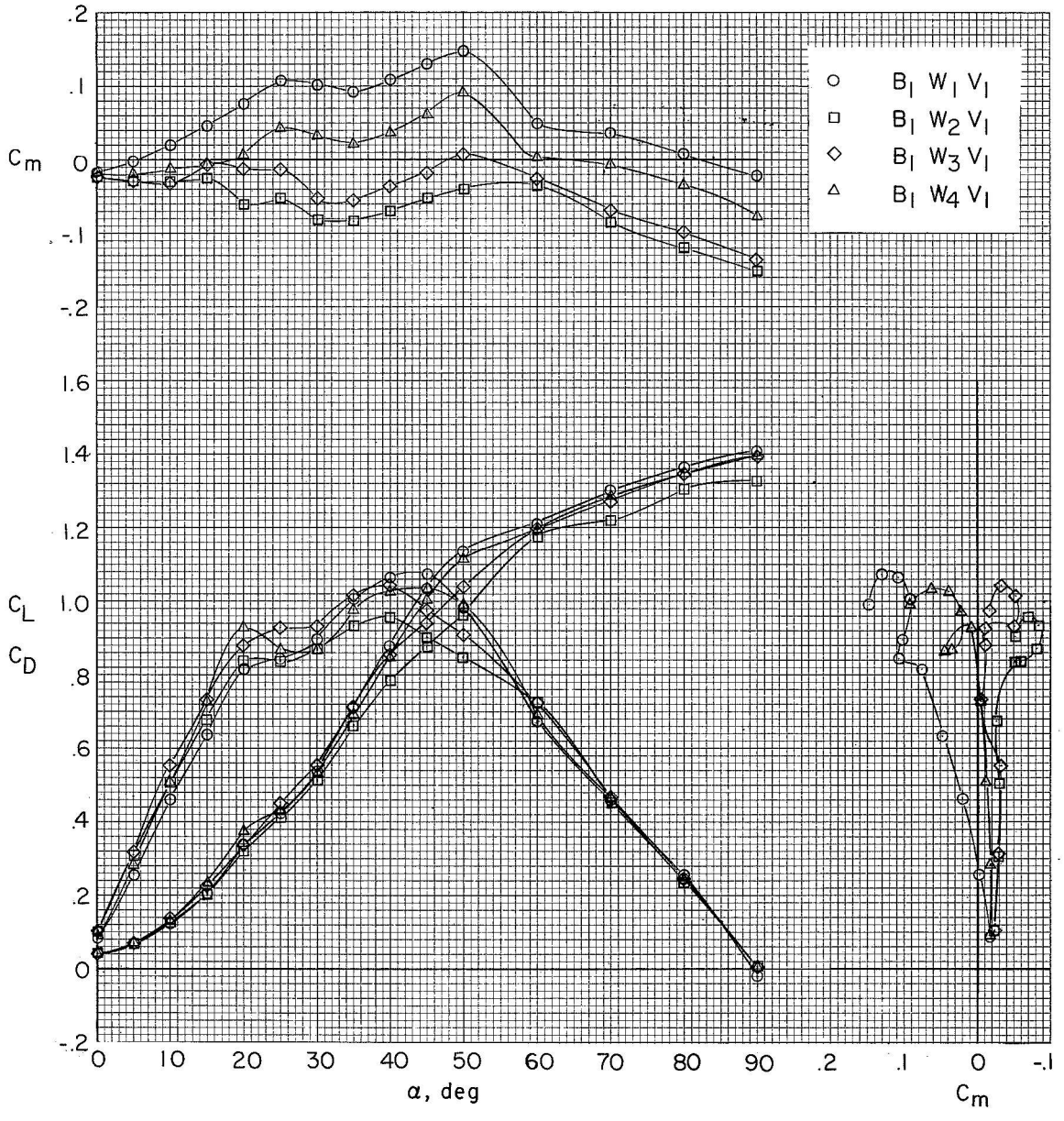

(a) Pitching moments referred to 64-percent-body station.

Figure 3.- Static longitudinal stability characteristics of the four configurations of the model used in the investigation. $\beta = 0^{\circ}$.

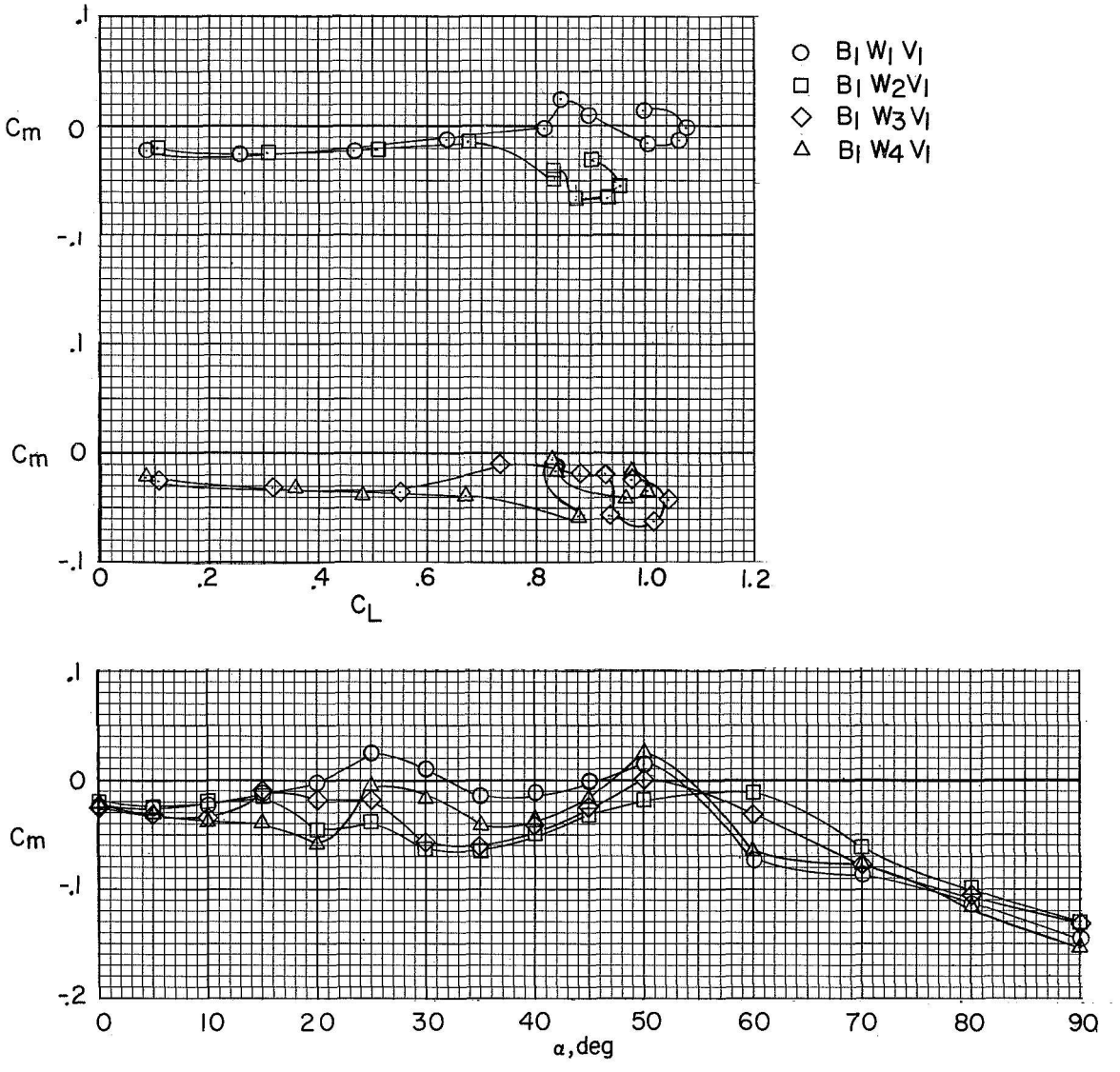

(b) Pitching moments referred to 40-percent-mean-aerodynamic chord of the individual wings.

Figure 3.- Concluded.

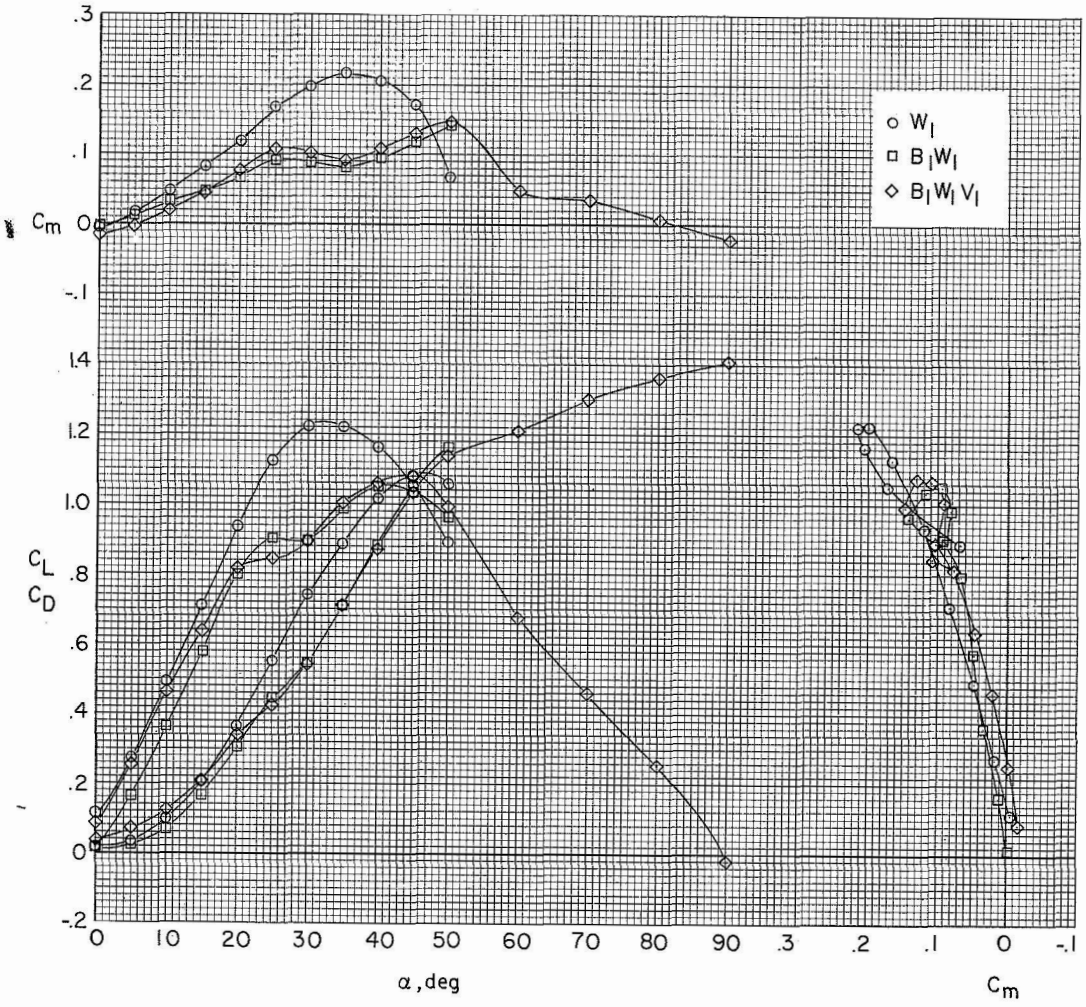

Figure 4.- Effect of model buildup on the static longitudinal stability characteristics of model $B_1W_1V_1$. $\beta = 0^\circ$.

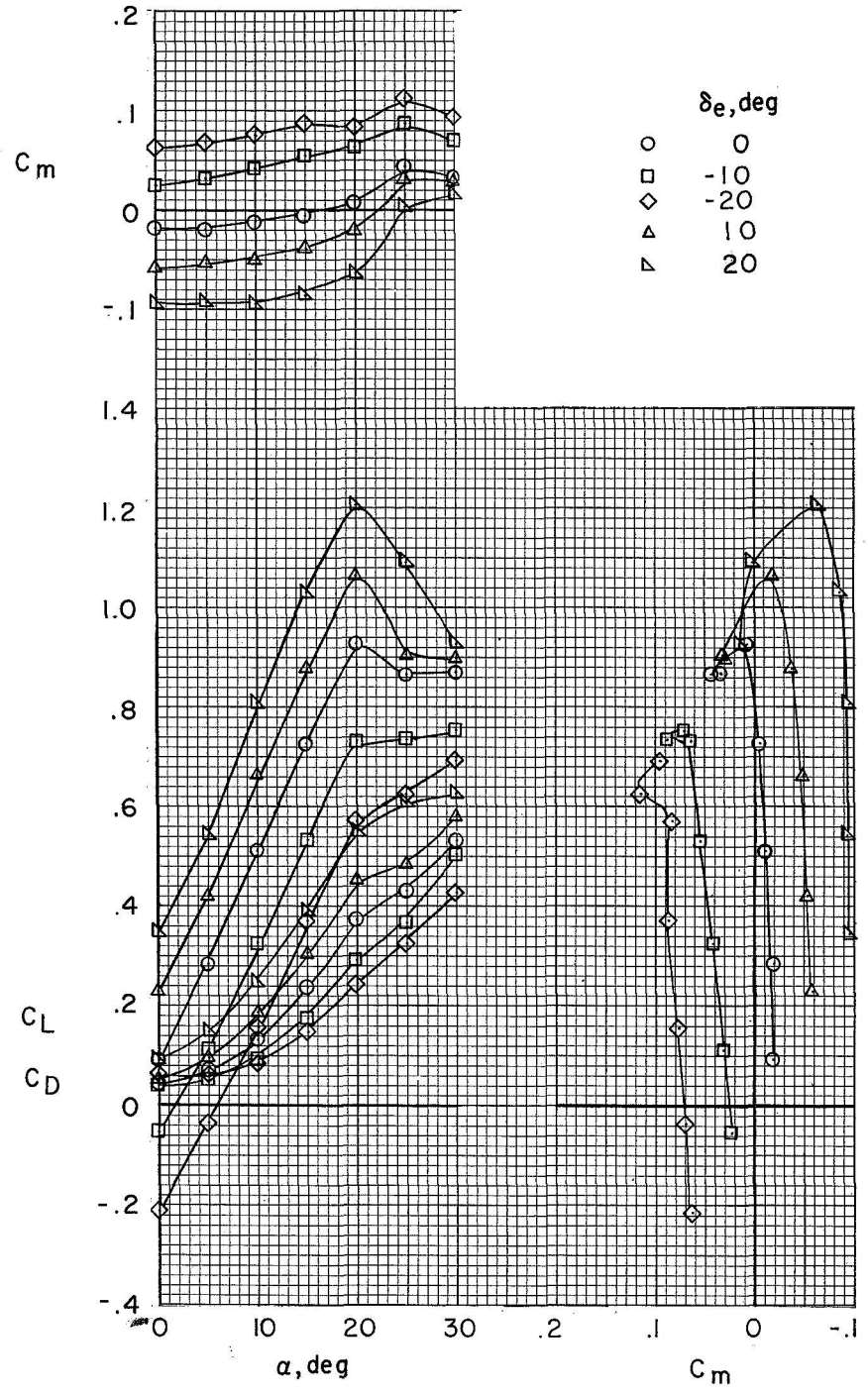

Figure 5.- Effect of elevator deflection on the static longitudinal stability characteristics of model $B_1W_4V_1$. $\beta = 0^\circ$.

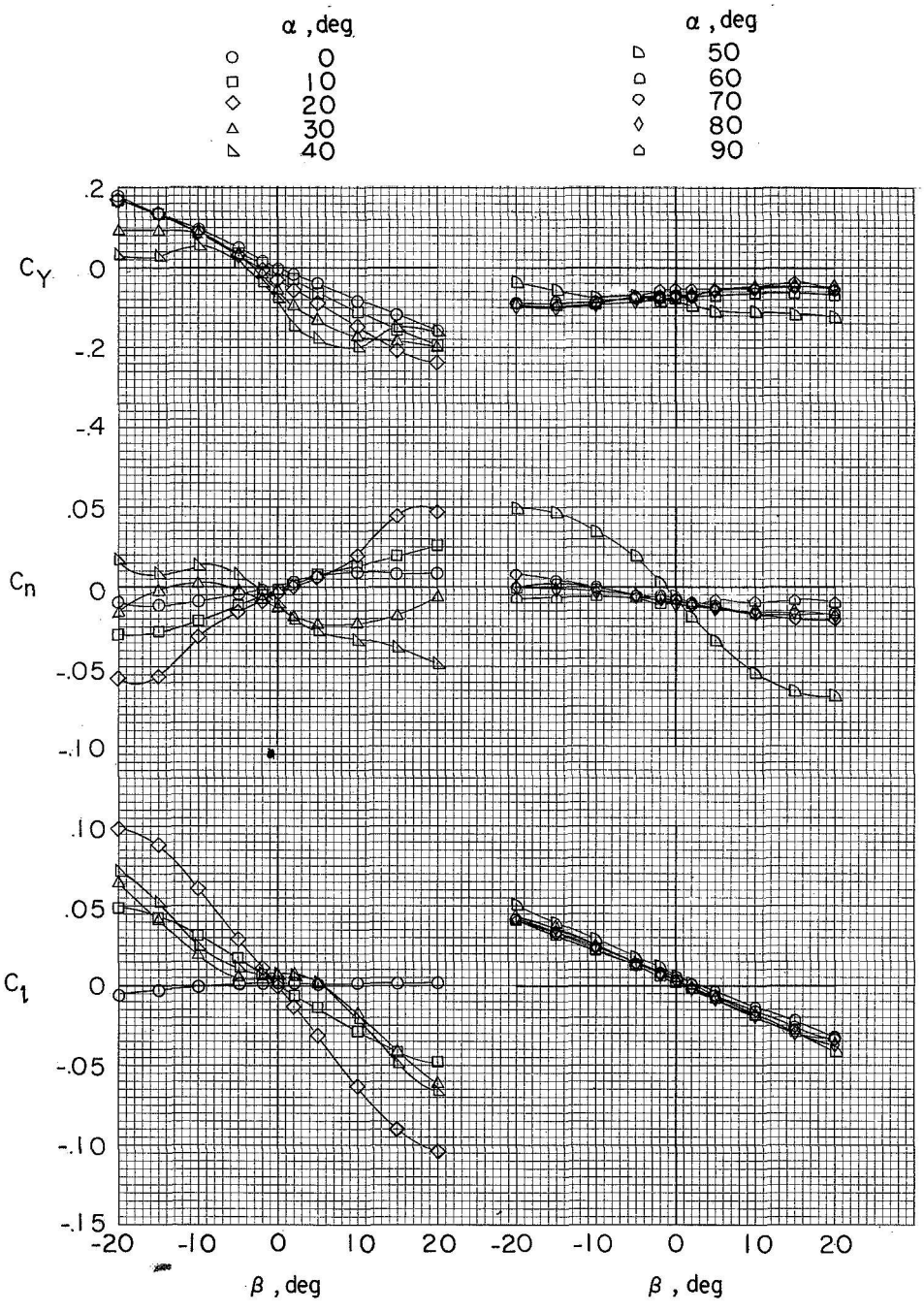

(a) Tails on.

Figure 6.- Variation of lateral coefficients of model $B_1W_1V_1$ with angle of sideslip. $\delta_e = 0^\circ$.

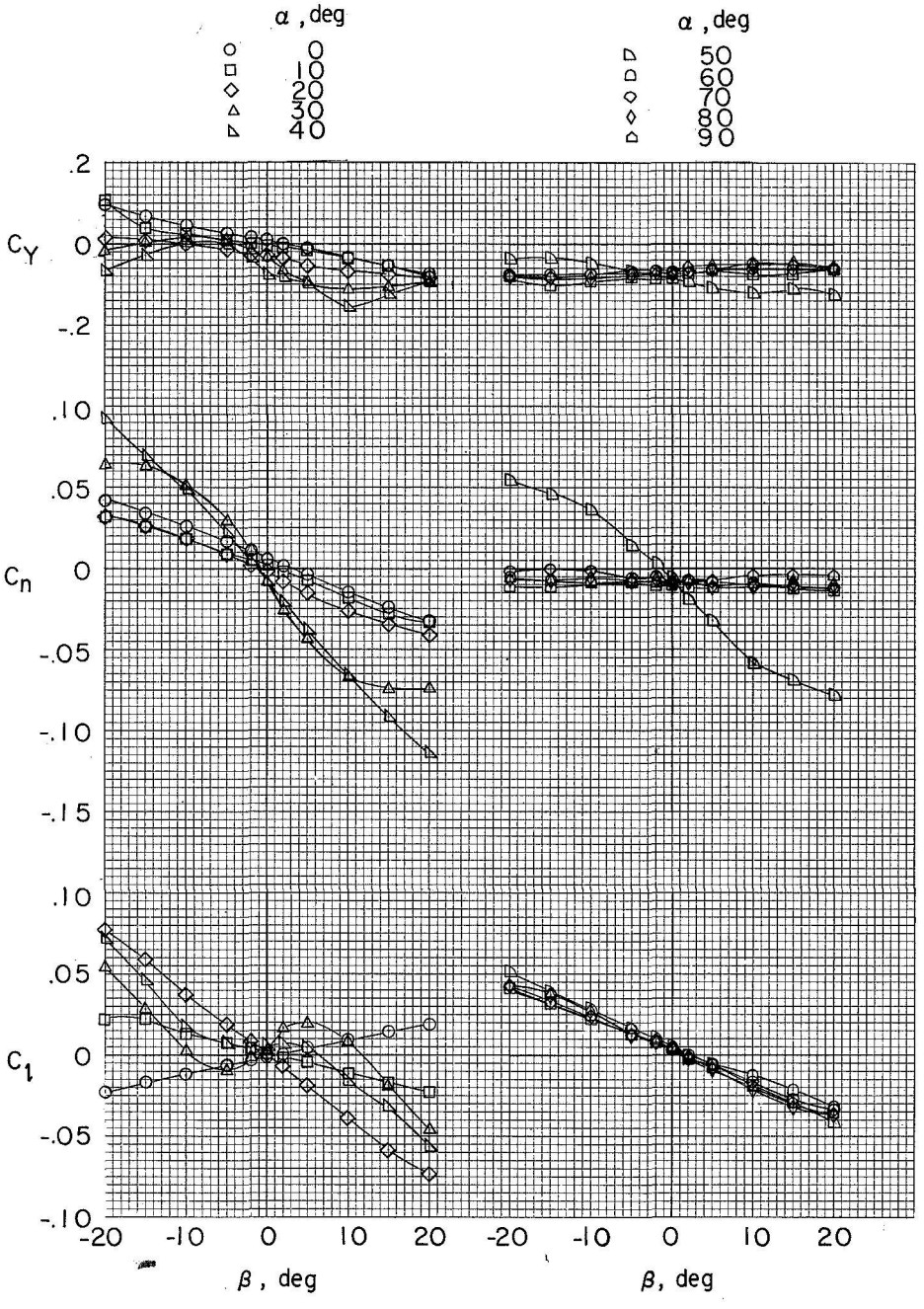

(b) Tails off (B_1W_1).

Figure 6.- Concluded.

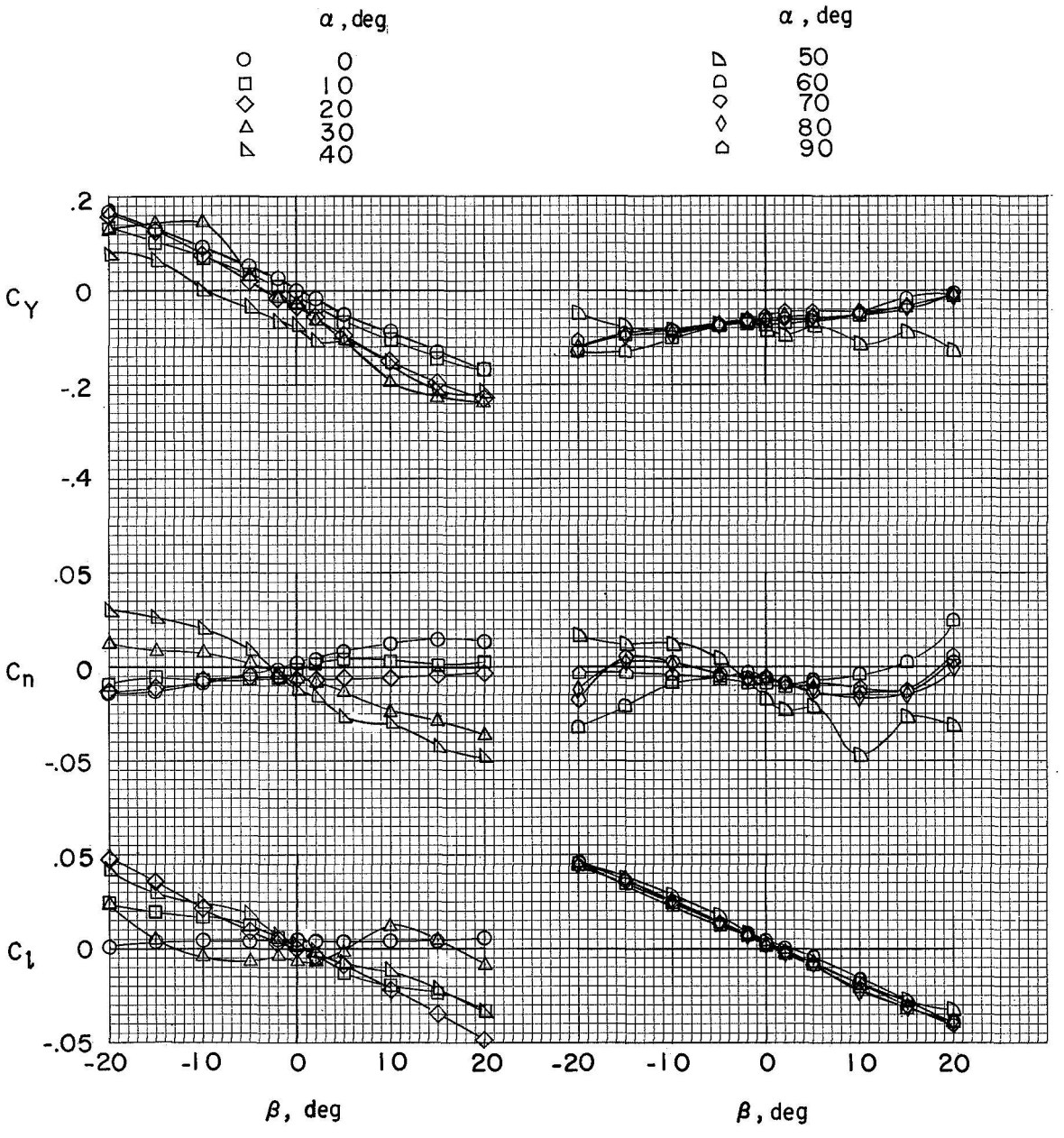

Figure 7.- Variation of lateral coefficients of model $B_1W_2V_1$ with angle of sideslip. $\delta_e = 0^o$.

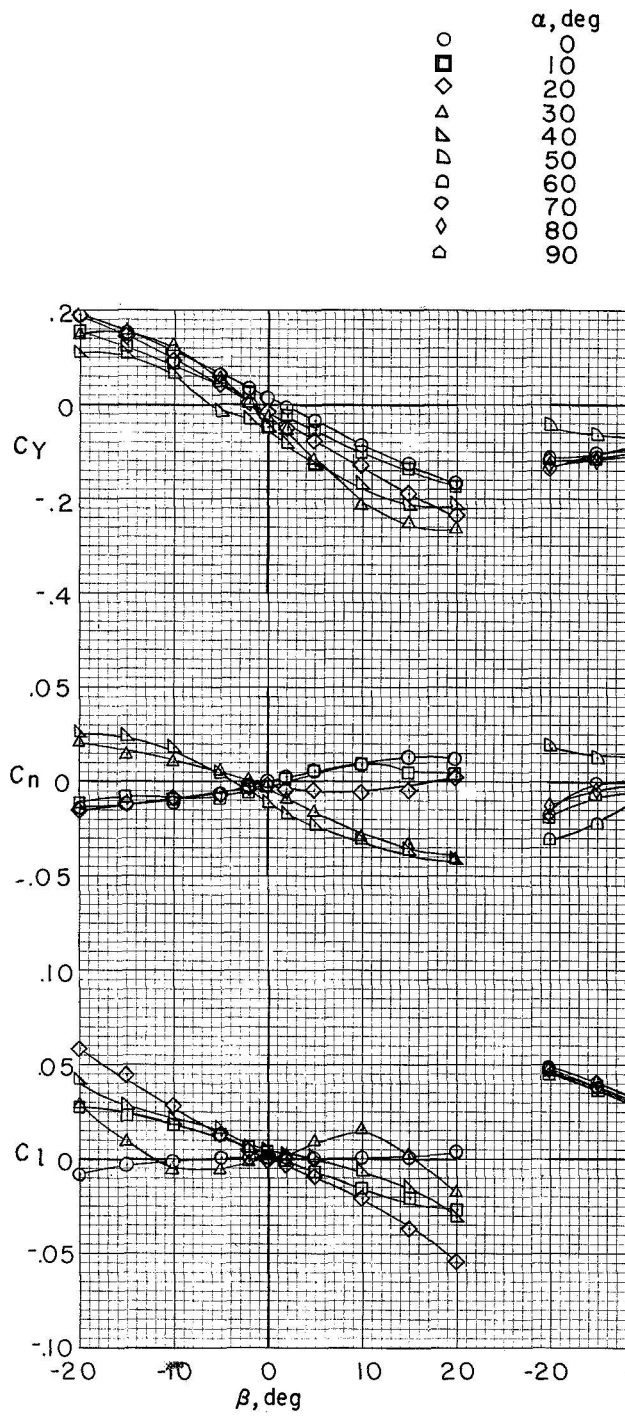

Figure 8.- Variation of lateral coefficients of model $B_1W_3V_1$ with angle of sideslip. $\delta_e = 0^o$.

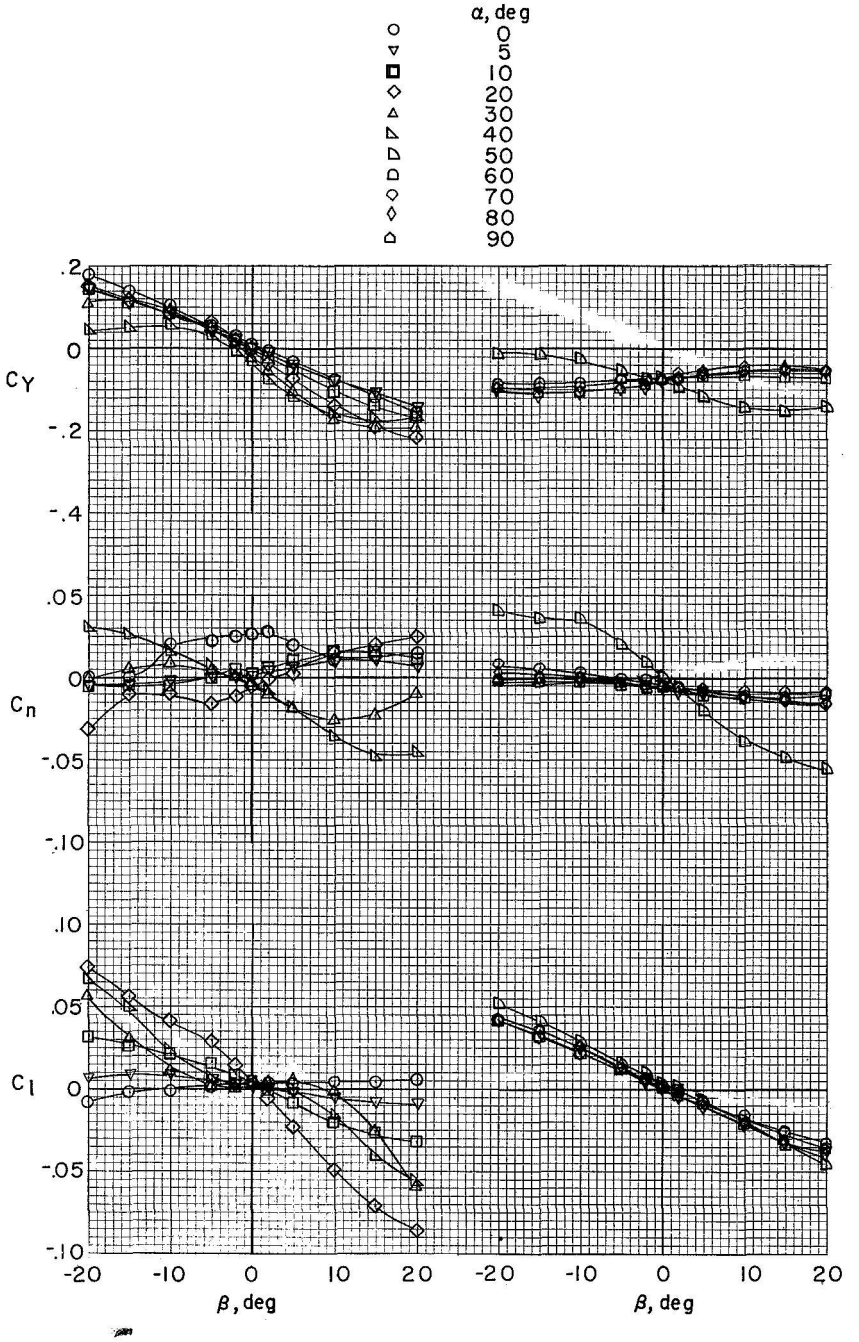

(a) Tails on.

Figure 9.- Variation of lateral coefficients of model $B_1W_4V_1$ with angle of sideslip. $\delta_e = 0^\circ$.

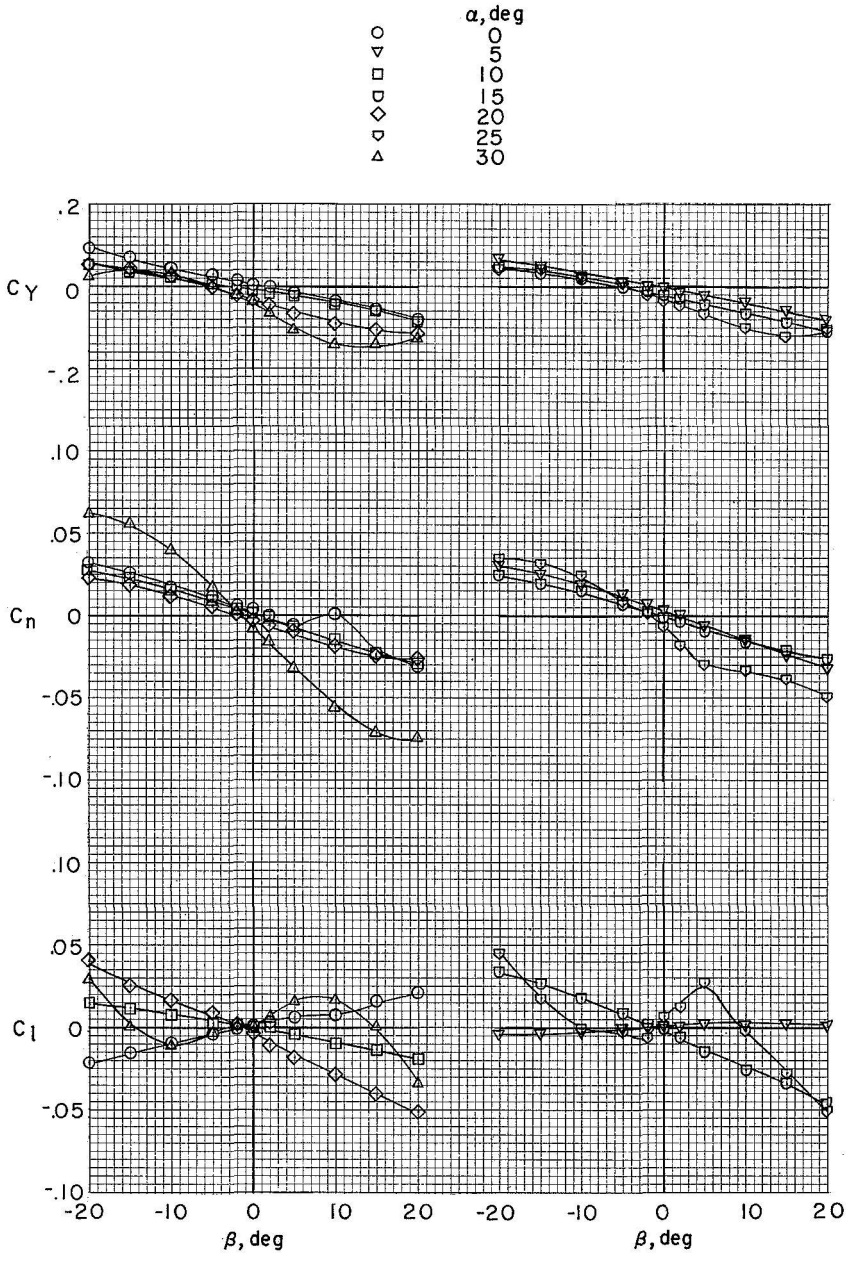

(b) Tails off (B_1W_4).

Figure 9.- Concluded.

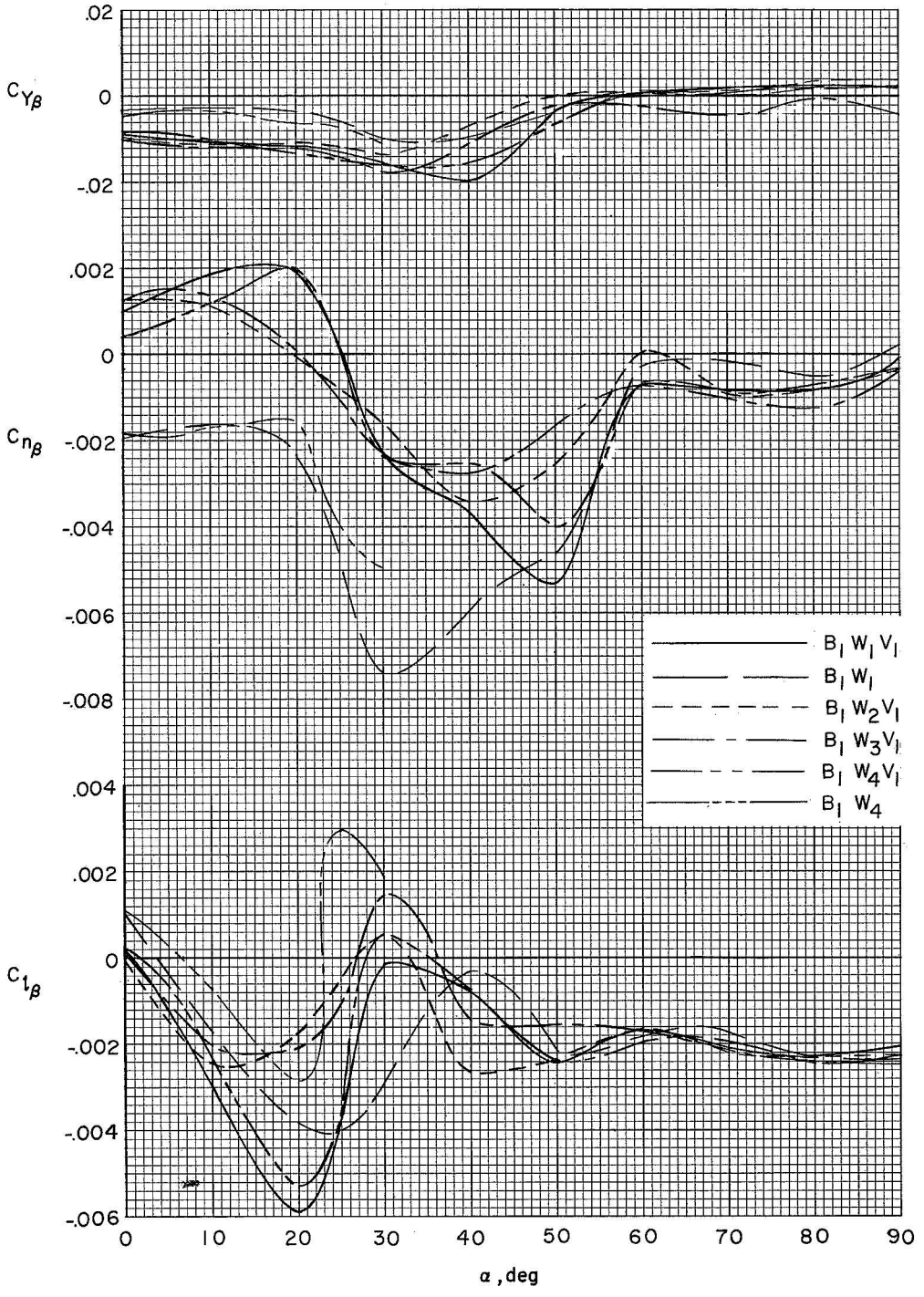

Figure 10.- Variation of static lateral stability derivatives with angle of attack. $\delta_e = 0^o$.

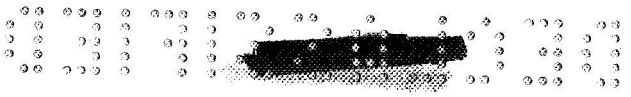

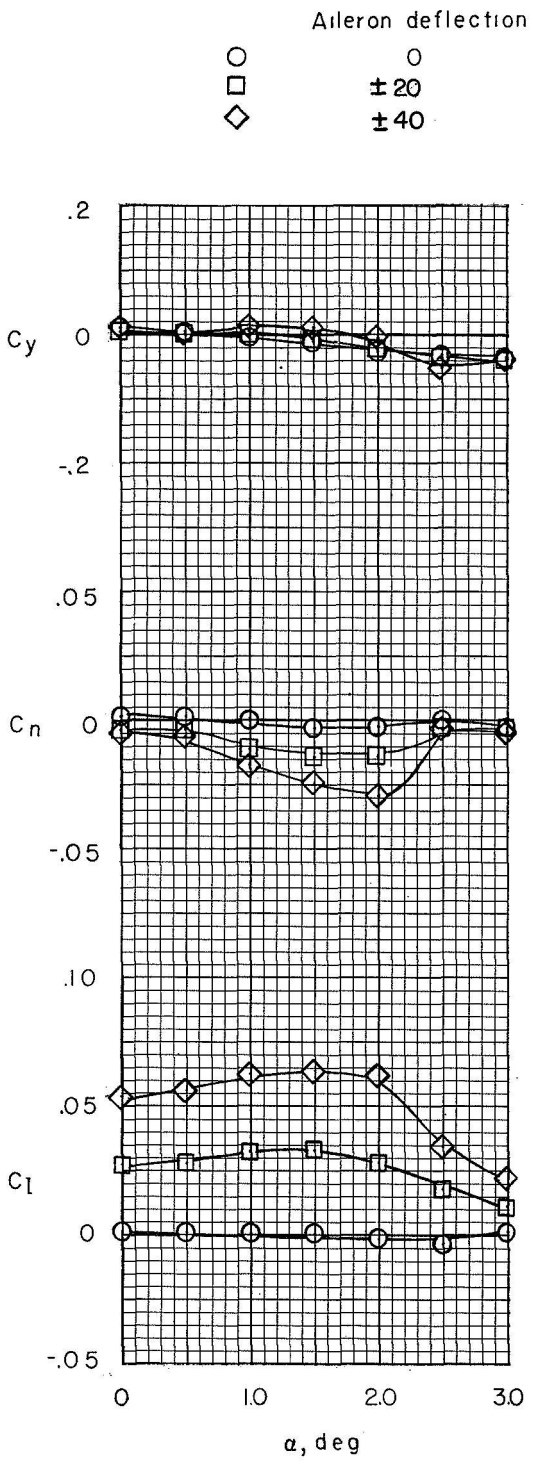

Figure 11.- Aileron effectiveness for model $B_1W_4V_1$. $\beta = 0^o$.

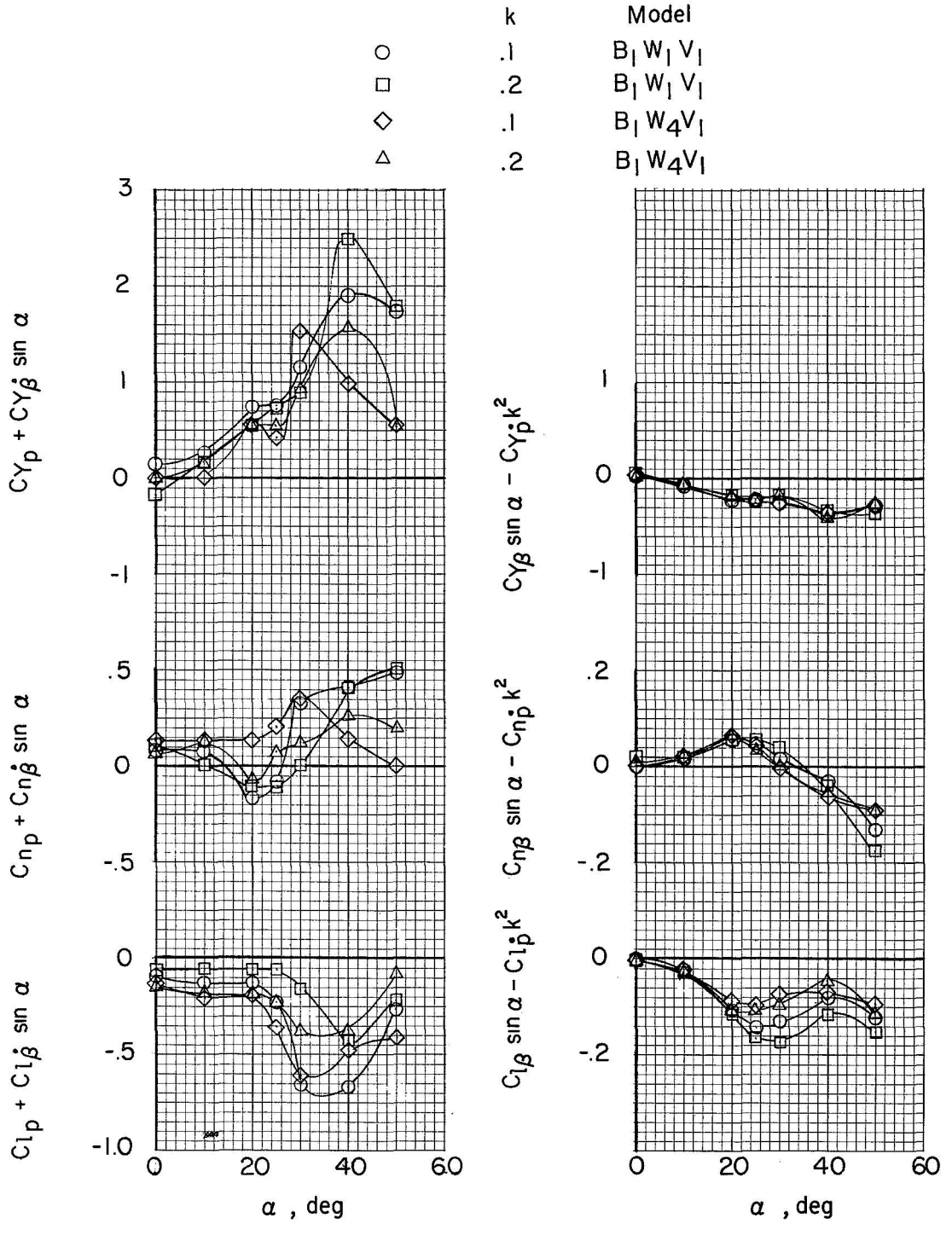

Figure 12.- Variation of out-of-phase and in-phase rolling derivatives with angle of attack for models $B_1W_1V_1$ and $B_1W_4V_1$.

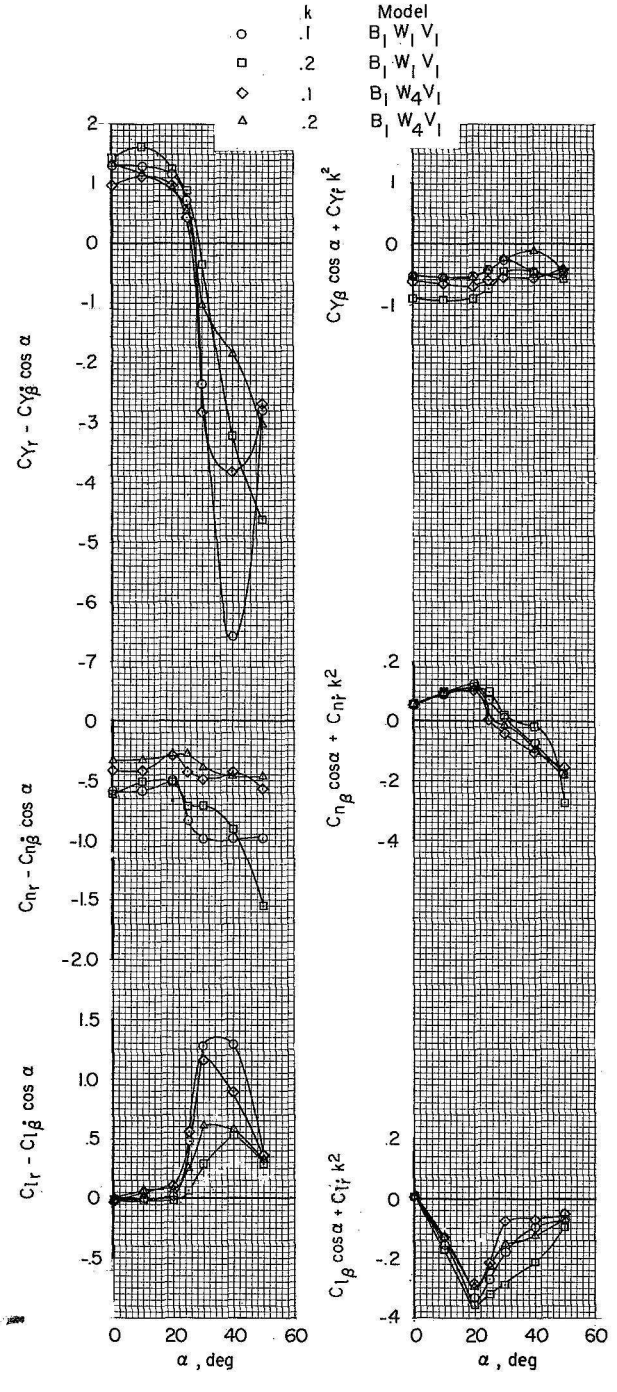

Figure 13.- Variation of out-of-phase and in-phase yawing derivatives with angle of attack for models $B_1W_1V_1$ and $B_1W_4V_1$.